Available online at www.sciencedirect.com
ScienceDirect
Comput. Methods Appl. Mech. Engrg. 289 (2015) 44–59
Computer methods in applied mechanics and engineering
www.elsevier.com/locate/cma

New analytical expressions in radial integration BEM for stress computation with several kinds of variable coefficients

Kai Yang*, Wei-Zhe Feng, Jun Li, Xiao-Wei Gao

State Key Laboratory of Structural Analysis for Industrial Equipment, Dalian University of Technology, Dalian 116024, China

Received 14 November 2014; received in revised form 2 February 2015; accepted 6 February 2015
Available online 14 February 2015

Abstract

This paper presents a set of new analytical expressions for evaluating radial integrals appearing in the stress computation of several kinds of variable coefficient elastic problems using the radial integration boundary element method (RIBEM). The strong singularity involved in the stress integral equation is explicitly removed from the derivation of the analytical expressions. This approach can improve the computational efficiency considerably and can overcome the time-consuming deficiency of RIBEM in computing involved radial integrals. In addition, because it can solve many kinds of variable coefficient elastic problems, this approach has a very wide applicability. The fourth-order spline (Radial Basis Function) RBF is employed to approximate the unknowns appearing in domain integrals caused by the variation of the shear modulus. The radial integration method is utilized to convert domain integrals to the boundary, which results in a pure boundary discretization algorithm. Numerical examples are given to demonstrate the efficiency of the presented formulations.

Keywords: Boundary element method; Radial integration method; Stress integral equation; Several kinds of variable coefficient

1. Introduction

The conventional boundary integral equations dealing with non-homogeneous and non-linear elastic problems [1,2] include domain integrals in the resulting integral equations. To evaluate these domain integrals, the computational region is required to be discretized into internal cells, which makes BEM lose its distinct advantage of only boundary discretization. To circumvent this deficiency, methods of transforming domain integrals into equivalent boundary integrals are proposed and have been frequently used. In these methods, the dual reciprocity method (DRM) developed by Brebbia [2] is extensively utilized. However, DRM requires particular solutions to basis functions, which restricts its application to complicated problems. Recently, a new transformation method, the radial integration method (RIM), has been developed by Gao [3,4], which not only can transform any complicated domain integrals to the boundary in a unified way without using particular solutions, but also can remove various singularities appearing

* Corresponding author.
E-mail address: kyang@dlut.edu.cn (K. Yang).

http://dx.doi.org/10.1016/j.cma.2015.02.007

in domain integrals [5,6]. Due to the advantages of RIM that particular solutions are not required and several domain integrals appearing in the same integral equation can be dealt with simultaneously, RIM-based boundary element method has won a good favor from many BEM researchers [7–10] in recent years. However, although the radial integration boundary element method (RIBEM) is very flexible to deal with the general non-linear and non-homogeneous problems [11,12], evaluation of the radial integrals numerically is very time-consuming compared to other methods [13,14], especially for large three-dimensional problems.

In this paper, a new type of boundary-only integral equation analysis technique is developed for several kinds of variable coefficient elastic stress computation based on the fundamental solutions of homogeneous problems. Unlike the existing method (e.g. [9]) which evaluates the radial integrals numerically, the method developed in this paper can analytically integrate the radial integrals by using the fourth-order spline radial basis function (RBF). The strong singularity involved in the stress integral equation [15] is explicitly removed from the derivation of the analytical expressions. Through use of the derived analytical expressions in RIBEM, the computational efficiency can be improved considerably. Three numerical examples are given to demonstrate the efficiency of the presented method, which show that approximately 80% computational time can be saved by using the analytical expressions than by using numerical method to compute the radial integrals. Though the formulations are derived on the elastic stress background, they can also be applied to other physical problems based on the use of RIBEM (e.g. [16–19]).

2. Review of non-homogeneous BEM in elastic problems [9]

Consider non-homogeneous and linear elastic solid materials. In the absence of body forces, the equilibrium equation is given by

$$\sigma_{jk,k} = 0 \tag{1}$$

where σ_{jk} represents the stress tensor, a comma ',' after a quantity represents spatial derivatives, and repeated indexes denote summation. It is assumed that the shear modulus μ of the material depends on Cartesian coordinates while Poisson's ratio ν is constant. Under this assumption, the stress tensor σ_{jk} and the displacement gradient $u_{k,l} = \partial u_k/\partial x_l$ are related by the following generalized Hooke's law:

$$\sigma_{ij} = C_{ijkl}u_{k,l} = \mu C^0_{ijkl}u_{k,l} \tag{2}$$

where C^0_{ijkl} is the elastic constitutive tensor [20]. The weak-form of the equilibrium equation (1) can be written as follows:

$$\int_\Omega U_{ij}\sigma_{jk,k}d\Omega = 0 \tag{3}$$

where U_{ij} is a weight function, which is taken as Kelvin's displacement fundamental solution in this paper. Substituting Eq. (2) into Eq. (3) and applying Gauss's divergence theorem yield [20]

$$c\tilde{u}_i(\boldsymbol{x}^p) = \int_\Gamma U_{ij}(\boldsymbol{x},\boldsymbol{x}^p)t_j(\boldsymbol{x})d\Gamma(\boldsymbol{x}) - \int_\Gamma T_{ij}(\boldsymbol{x},\boldsymbol{x}^p)\tilde{u}_j(\boldsymbol{x})d\Gamma(\boldsymbol{x}) + \int_\Omega V_{ij}(\boldsymbol{x},\boldsymbol{x}^p)\tilde{u}_j(\boldsymbol{x})d\Omega(\boldsymbol{x}) \tag{4}$$

where $c = 1$ for internal points and $c = 0.5$ for smooth boundary nodes. The fundamental solutions U_{ij} and T_{ij} appearing in Eq. (4) can be found in usual elasticity BEM book, e.g. [20] and the kernel function V_{ij} can be expressed as follows:

$$V_{ij} = \frac{-1}{4\pi\alpha(1-\nu)r^\alpha}\left\{r_{,k}\tilde{\mu}_{,k}[(1-2\nu)\delta_{ij} + \beta r_{,i}r_{,j}] + (1-2\nu)(\tilde{\mu}_{,i}r_{,j} - \tilde{\mu}_{,j}r_{,i})\right\} \tag{5}$$

in which, $\beta = 2$ (2D) or $\beta = 3$ (3D), and $\alpha = \beta - 1$. $\tilde{u}_j$ and $\tilde{\mu}$ are the normalized displacements and shear modulus defined as follows:

$$\begin{aligned}\tilde{u}_j &= \mu u_j\\ \tilde{\mu} &= \ln\mu.\end{aligned} \tag{6}$$

From the first expression of Eq. (6), it follows that

$$\frac{\partial u_i}{\partial x_j^p} = \frac{1}{\mu}\left(\frac{\partial \tilde{u}_i}{\partial x_j^p} - \tilde{u}_i \frac{\partial \tilde{\mu}}{\partial x_j^p}\right). \tag{7}$$

Taking the partial derivative of Eq. (4) with respect to the source point x^p, and then substituting the result into Eq. (7) and making use of Eq. (2), we can obtain the following stress integral equation.

$$\begin{aligned}\sigma_{ij}(\boldsymbol{x}^p) = &\int_\Gamma U_{ijk}(\boldsymbol{x},\boldsymbol{x}^p)t_k(\boldsymbol{x})d\Gamma(\boldsymbol{x}) - \int_\Gamma T_{ijk}(\boldsymbol{x},\boldsymbol{x}^p)\tilde{u}_k(\boldsymbol{x})d\Gamma(\boldsymbol{x})\\ &+ \int_\Omega V_{ijk}(\boldsymbol{x},\boldsymbol{x}^p)\tilde{u}_k(\boldsymbol{x})d\Omega(\boldsymbol{x}) + F_{ijk}(\boldsymbol{x}^p)\tilde{u}_k(\boldsymbol{x}^p)\end{aligned} \tag{8}$$

in which the kernel functions U_{ijk} and T_{ijk} are the same as given in usual BEM books (e.g., [20]), and other quantities are as follows:

$$\begin{aligned}V_{ijk} = &\frac{1}{2\pi\alpha(1-v)}\frac{1}{r^\beta}\{\beta\tilde{\mu}_{,m}r_{,m}[(1-2v)\delta_{ij}r_{,k} + v(\delta_{ik}r_{,j} + \delta_{jk}r_{,i}) - \gamma r_{,i}r_{,j}r_{,k}]\\ &+ \beta v(\tilde{\mu}_{,i}r_{,j} + \tilde{\mu}_{,j}r_{,i})r_{,k} + (1-2v)(\beta\tilde{\mu}_{,k}r_{,i}r_{,j} + \tilde{\mu}_{,j}\delta_{ik} + \tilde{\mu}_{,i}\delta_{jk}) - (1-4v)\tilde{\mu}_{,k}\delta_{ij}\}\end{aligned} \tag{9}$$

$$F_{ijk} = \begin{cases}\dfrac{-1}{4(1-v)}((\delta_{ij}\tilde{\mu}_{,k} + \delta_{ik}\tilde{\mu}_{,j} + \delta_{jk}\tilde{\mu}_{,i})) & \text{for 2D}\\ \dfrac{-1}{15(1-v)}((2+10v)\delta_{ij}\tilde{\mu}_{,k} + (7-5v)(\delta_{ik}\tilde{\mu}_{,j} + \delta_{jk}\tilde{\mu}_{,i})) & \text{for 3D.}\end{cases} \tag{10}$$

3. Transformation of domain integrals to the boundary by RIM

To avoid discretizing the computational domain into cells in evaluating the domain integrals appearing in Eqs. (4) and (8), the radial integration method (RIM) [3–6] is applied to convert these domain integrals into equivalent boundary integrals and results in a boundary-only discretization algorithm. However, since the normalized displacement $\tilde{\mu}_k(\boldsymbol{x})$ appearing in Eqs. (4) and (8) is unknown, the RIM formulations cannot be directly evaluated. To solve this problem, the unknowns are approximated by a series of prescribed radial basis functions (RBFs). Thus,

$$\tilde{u}_i(\boldsymbol{x}) = \sum_A \alpha^A \phi^A(R) + a^k x_k + a^0 \tag{11}$$

$$\sum_A \alpha^A = 0, \qquad \sum_A \alpha^A x_i^A = 0 \tag{12}$$

in which, $R = \|\boldsymbol{x} - \boldsymbol{x}^A\|$ is the distance from the application point $\boldsymbol{x}^A$ to the field point $\boldsymbol{x}$, α^A and a^k are coefficients to be determined by nodal displacement values through a node allocation scheme, and ϕ^A is the radial basis function. Numerical investigation indicates that the 4th order spline-type radial basis function can give very stable results [9], its expression being as follows:

$$\phi^A(R/d_A) = \begin{cases}1 - 6\left(\dfrac{R}{d_A}\right)^2 + 8\left(\dfrac{R}{d_A}\right)^3 - 3\left(\dfrac{R}{d_A}\right)^4 & 0 \le R \le d_A\\ 0 & R \ge d_A\end{cases} \tag{13}$$

where, d_A is the support size for the application point A. Substituting Eq. (11) into the domain integral of Eqs. (4) and (8) and applying RIM formulations [3–6] yield

$$\int_\Omega V_{ij}\tilde{u}_j d\Omega = \sum_A \alpha_j^A \int_\Gamma \frac{1}{r^\alpha}\frac{\partial r}{\partial n}F_{ij}^A d\Gamma + a_j^k \int_\Gamma \frac{r_{,k}}{r^\alpha}\frac{\partial r}{\partial n}F_{ij}^1 d\Gamma \tag{14}$$

$$F_{ij}^A = \int_0^r r^\alpha V_{ij}\phi^A dr \tag{15}$$

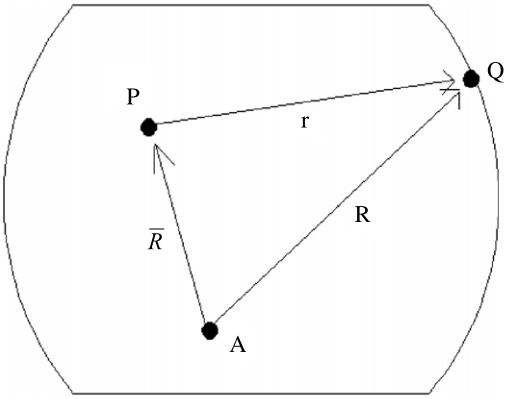

Fig. 1. Relationship between distances.

$$F_{ij}^{1} = \int_0^r r^{\beta} V_{ij} dr \tag{16}$$

and

$$\int_{\Omega} V_{ijk} \tilde{u}_k d\Omega = \sum_A \alpha_k^A \int_{\Gamma} \frac{1}{r^{\alpha}} \frac{\partial r}{\partial n} F_{ijk}^A d\Gamma + a_k^l \int_{\Gamma} \frac{r_{,l}}{r^{\alpha}} \frac{\partial r}{\partial n} F_{ijk}^1 d\Gamma \tag{17}$$

$$F_{ijk}^{A} = \int_0^r r^{\alpha} V_{ijk} \phi^A dr \tag{18}$$

$$F_{ijk}^{1} = \int_0^r r^{\beta} V_{ijk} dr. \tag{19}$$

To evaluate the radial integrals shown in Eqs. (15) and (18), referring to Fig. 1, the following relationships are used:

$$R = \sqrt{r^2 + 2sr + \bar{R}^2}, \qquad S = r_{,i} \bar{R}_i, \qquad \bar{R}_i = x_i^p - x_i^A. \tag{20}$$

From Eq. (5), it can be seen that the radial integrals in Eq. (15) are regular and can be integrated without any difficulty. However, from Eq. (9) we can see that the radial integrals for F_{ijk}^A in Eq. (18) are strongly singular with the order of $(1/r)$ when the source point approaches the field point. Therefore, a special technique, referred as singularity separation technique, is required to evaluate these radial integrals.

4. Analytical expressions for evaluation of radial integrals in stress computation

The radial integrals shown by Eqs. (15)–(19) can be evaluated analytically or numerically by using the following variable transformation relationship:

$$x_i = y_i + r_{,i} r \tag{21}$$

where, x_i and y_i are the coordinates of source point and field point respectively, and $r_{,i} = \partial r / \partial x_i$.

It is noted that $r_{,i}$ and y_i are constants for the radial integral. This is an important characteristic of RIM, which makes the evaluation of the radial integrals in Eqs. (15)–(19) possible and easy for any complicated function.

Using the conventional singularity separation scheme, Eq. (18) can be rewritten as follows:

$$F_{ijk}^{A} = \int_0^r r^{\alpha} V_{ijk} \phi^A dr = \int_0^r r^{\alpha} V_{ijk} \left(\phi^A(R) - \phi^A(0) \right) dr + \int_0^r r^{\alpha} V_{ijk} \phi^A(0) dr \tag{22}$$

where $\phi^A(0)$ is the expression when $r = 0$.

Table 1
Three kinds of variable shear modulus.

	Case 1 (exponential change of linear order)	Case 2 (linear)	Case 3 (exponential change of secondary order)
μ	$\mu_0 e^{c_i x_i}$	$\mu_0 + c_i x_i$	$\mu_0 e^{c_0 + c_i x_i + c_{ij} x_i x_j}$
$\tilde{\mu}$	$\ln \mu_0 + c_i x_i$	$\ln(\mu_0 + c_i x_i)$	$\ln \mu_0 + c_0 + c_i x_i + c_{ij} x_i x_j$
$\tilde{\mu}_{,i}$	c_i	$\frac{c_i}{\mu_0 + c_j x_j}$	$c_i + c_{jk}(\delta_{ij} x_k + \delta_{ik} x_j)$

Considering $r_{,i}$ is constant in the radial integral, according to the expression of kernel function Eqs. (5) and (9), Eq. (16) can be easily derived and Eqs. (15) and (18) can include radial integral of the following categories:

$$F^1_{ijk} \to \int_0^r \tilde{\mu}_{,i} dr \tag{23a}$$

$$F^A_{ij} \to \int_0^r \phi^A(R) \tilde{\mu}_{,i} dr \tag{23b}$$

$$F^A_{ijk} \to \int_0^r \frac{\phi^A(R) - \phi^A(0)}{r} \tilde{\mu}_{,i} dr, \qquad \int_0^r \frac{\tilde{\mu}_{,i}}{r} dr. \tag{23c}$$

Using a numerical integral formula to calculate the radial integral is usually very time-consuming, especially for large three-dimensional problems. If we can evaluate these integrals in an analytical method, it can greatly improve the computational efficiency. Here are the analytical expressions of the three kinds of representative variable shear modulus as shown in Table 1.

For the above-mentioned shear modulus change forms, the following gives the analytical calculation formula of the radial basis function based on Table 1.

4.1. The radial integral analytical expressions of $F^1_{ijk} \to \int_0^r \tilde{\mu}_{,i} dr$

Using Eq. (21), the integral $F^1_{ijk} \to \int_0^r \tilde{\mu}_{,i} dr$ from Eq. (23a) can be easily derived as follows:

For case 1:

$$\int_0^r \tilde{\mu}_{,i} dr = c_i r. \tag{24}$$

For case 2:

$$\tilde{\mu}_{,i} = \frac{c_i}{\mu_0 + c_j x_j^p + c_j r_{,j} r} \tag{25}$$

$$\int_0^r \tilde{\mu}_{,i} dr = \frac{c_i \ln(\mu_0 + c_j x_j)}{c_j r_{,j}} = \frac{c_i \ln \mu}{c_j r_{,j}}. \tag{26}$$

For case 3:

$$\tilde{\mu}_{,i} = c_i + c_{jk}(\delta_{ij} x_k^p + \delta_{ik} x_j^p) + c_{jk}(\delta_{ij} r_{,k} + \delta_{ik} r_{,j}) r \tag{27}$$

$$\int_0^r \tilde{\mu}_{,i} dr = [c_i + c_{jk}(\delta_{ij} x_k^p + \delta_{ik} x_j^p)] r + \frac{1}{2} c_{jk}(\delta_{ij} r_{,k} + \delta_{ik} r_{,j}) r^2. \tag{28}$$

4.2. The radial integral analytical expressions of $F^A_{ijk} \to \int_0^r \frac{\tilde{\mu}_{,i}}{r} dr$

Similarly, using Eq. (21), the integral $\int_0^r \frac{\tilde{\mu}_{,i}}{r} dr$ from Eq. (23c) can be derived as follows:

For case 1:

$$\int_0^r \frac{\tilde{\mu}_{,i}}{r} dr = c_i \ln r. \tag{29}$$

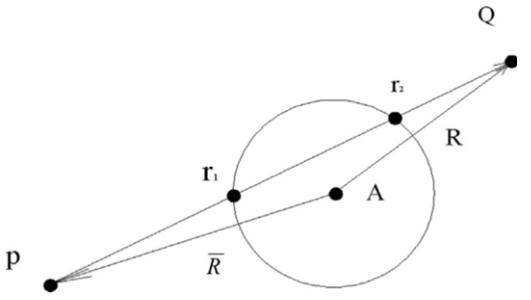

Fig. 2. Intersections between line and circle.

For case 2:

Referring to Eq. (25), it follows:

$$\int_0^r \frac{\tilde{\mu}_{,i}}{r} dr = \frac{c_i}{\mu_0 + c_j x_j^p} \ln\left(\frac{r}{\mu}\right). \tag{30}$$

For case 3:

Referring to Eq. (27), it follows:

$$\int_0^r \frac{\tilde{\mu}_{,m}}{r} dr = [c_m + c_{ij}(\delta_{im} x_j^p + \delta_{jm} x_i^p)] \ln r + c_{ij}(\delta_{im} r_{,j} + \delta_{jm} r_{,i}) r. \tag{31}$$

4.3. The radial integral analytical expressions of $F_{ij}^A \to \int_0^r \phi^A(R)\tilde{\mu}_{,i} dr$

Using Eq. (21), the integral $F_{ij}^A \to \int_0^r \phi^A(R)\tilde{\mu}_{,i} dr$ from Eq. (23b) can be derived as follows:

For case 1: (exponential change of linear order)

Since $\tilde{\mu}_{,i} = c_i$ is constant for $\mu = \mu_0 e^{c_i x_i}$, the integral can be rewritten as follows: $\Psi_1 = \int_0^r \phi^A dr$, referring to Ref. [16] and based on Eqs. (14) and (20), it can be derived that:

$$\begin{aligned}
\Psi_1 = \int_0^r \phi^A dr &= \int_{r_1}^{r_2} \left\{1 - 6\left(\frac{R}{d_A}\right)^2 + 8\left(\frac{R}{d_A}\right)^3 - 3\left(\frac{R}{d_A}\right)^4\right\} \mathrm{d}r \\
&= r - \left[\frac{3}{5}r^5 - 3sr^4 - 2r^3(\bar{R}^2 + 2s^2) - 6sr^2\bar{R}^2 - 3r\bar{R}^4\right]/d_A^4 + \\
&\quad [(r+s)(2r^2 + 5\bar{R}^2 + 4rs - 3s^2)\sqrt{r^2 + 2sr + \bar{R}^2} + 3(\bar{R}^2 - s^2)^2 \\
&\quad \log(r + s + \sqrt{r^2 + 2sr + \bar{R}^2})]/d_A^3 - (2r^3 - 6sr^2 - 6\bar{R}^2 r)/d_A^2 \Big|_{r_1}^{r_2}
\end{aligned} \tag{32}$$

where r_1 and r_2 are the intersections between the line r and the circle centered at A with radius of d_A, as shown in Fig. 2.

For case 2: (linear)

Referring to Eq. (25), and let $a = \mu_0 + c_j x_j^p$, $b = c_j r_{,j}$ and then referring to Fig. 2, the radial integral can be derived based on Eqs. (14) and (20) that:

$$\begin{aligned}
\int_0^r \phi^A(R)\tilde{\mu}_{,i} dr = \frac{c_i}{12b^5 d_A^4} &(-9b^4 r^4 + 12b^3 r^3(a - 4bs) + 36br(a - 2bs)(a^2 + 2b^2(d_A^2 + \bar{R}^2) - 2abs) \\
&- 18b^2 r^2(a^2 - 4abs + 2b^2(d_A^2 + \bar{R}^2 + 2s^2)) + 16b^2 d_A R(6a^2 - 3ab(r + 5s) \\
&+ b^2(8\bar{R}^2 + 2r^2 + 7rs + 3s^2)) + 12(-3a^4 + b^4(d_A^4 - 6d_A^2\bar{R}^2 - 3\bar{R}^4) \\
&+ 12a^3 bs + 12ab^3 s(d_A^2 + \bar{R}^2) - 6a^2 b^2(d_A^2 + \bar{R}^2 + 2s^2)) \ln(a + br) \\
&- 48bd_A(a - bs)(2a^2 - 4abs + b^2(3\bar{R}^2 - s^2)) \ln\left(r + s + \sqrt{r^2 + 2sr + \bar{R}^2}\right)
\end{aligned}$$

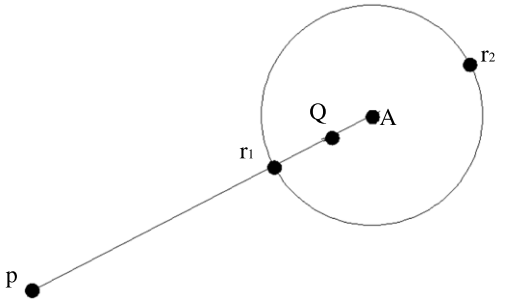

Fig. 3. A special intersection.

$$+96bd_A(a^2+b^2\bar{R}^2-2abs)^{\frac{3}{2}}(\ln(a+br)-\ln(b(\bar{R}^2+rs)$$
$$-a(r+s)+\sqrt{r^2+2sr+\bar{R}^2}\sqrt{a^2+b^2\bar{R}^2-2abs}))). \tag{33}$$

For the expression as shown in Eq. (33), it should be noted that a special case, $r+s+\sqrt{r^2+2sr+\bar{R}^2}=0$, may occur. In this case, $s=-\bar{R}$, as shown in Fig. 3, and $F_{ij}^A \to \int_0^r \phi^A(R)\tilde{\mu}_{,i}dr$ can be integrated as follows:

$$\begin{aligned}\int_0^r \phi^A(R)\tilde{\mu}_{,i}dr = {} & \frac{c}{12b^5d_A^4(r-\bar{R})}(br(36a^3(r-k)-6a^2b(24\bar{R}^2-16d_A|\bar{R}-r|-27\bar{R}r+3r^2)\\
&+12ab^2(24\bar{R}^2r-18\bar{R}^3-4d_A(|\bar{R}-r|)(r-6\bar{R})-7\bar{R}r^2+r^3+6d_A^2(r-\bar{R}))\\
&+b^3(-36d_A^2(4\bar{R}^2-5\bar{R}r+r^2)+16d_A(|\bar{R}-r|)(18\bar{R}^2-9\bar{R}r+2r^2)\\
&-3(48\bar{R}^4-84\bar{R}^3r+52\bar{R}^2r^2-19\bar{R}r^3+3r^4)))\\
&+12(3a-bd_A+3b\bar{R})(a+b(d_A+\bar{R}))^3(\bar{R}-r)\ln(a+br)).\end{aligned} \tag{34}$$

For case 3: (exponential change of secondary order)

Referring to Eq. (27) and let $a=c_i+c_{jk}(\delta_{ij}x_k^p+\delta_{ik}x_j^p)$, $b=c_{jk}(\delta_{ij}r_{,k}+\delta_{ik}r_{,j})$ then referring to Fig. 2 and based on Eqs. (14) and (20), it can be derived that:

$$\begin{aligned}\int_0^r \phi^A(R)\tilde{\mu}_{,i}dr = {} & \frac{1}{10d_A^4}\Big(2a(5d_A^4r+5d_A(r+s)R(5\bar{R}^2+2r^2+4rs-3s^2)-10d_A^2r(3\bar{R}^2+r(r+3s))\\
&-r(15d_A^4+10d_A^2r(r+3s)+r^2(3r^2+15rs+20s^2)))+b(5d_A^4r^2+2d_AR(8(\bar{R}^2+r^2)^2\\
&+r(7\bar{R}^2+22r^2)s+(2r^2-25\bar{R}^2)s^2-5rs^3+15s^4)\\
&-5\bar{R}^2r^2(6\bar{R}^2+r(3r+8s))-r^2(15\bar{R}^4+5\bar{R}^2r(3r+8s)+r^2(5r^2+24rs+30s^2)))\\
&+30d_A(a-bs)(\bar{R}^2-s^2)^2\ln\left(r+s+\sqrt{r^2+2sr+\bar{R}^2}\right)\Big).\end{aligned} \tag{35}$$

Similarly, for the expression as shown in Eq. (35), it should be noted that a special case, $r+s+\sqrt{r^2+2sr+\bar{R}^2}=0$, may occur. In this case, $s=-\bar{R}$, as shown in Fig. 3, and $F_{ij}^A \to \int_0^r \phi^A(R)\tilde{\mu}_{,i}dr$ can be integrated as follows:

$$\begin{aligned}\int_0^r \phi^A(R)\tilde{\mu}_{,i}dr = {} & \frac{-1}{10d_A^4}((\bar{R}-r)(10d_A^4(a+b\bar{R})-20d_A^2(a+b\bar{R})(\bar{R}-r)^2+15bd_A^2(\bar{R}-r)^3\\
&-6(a+b\bar{R})(\bar{R}-r)^4+5b(\bar{R}-r)^5+5bd_A^4(r-\bar{R})\\
&+4d_A(|\bar{R}-r|^3(5a+b(\bar{R}+4r)))).\end{aligned} \tag{36}$$

4.4. The radial integral analytical expressions of $F_{ijk}^A \to \int_0^r \frac{\phi^A(R)-\phi^A(0)}{r}\tilde{\mu}_{,i}dr$

Similarly also, using Eq. (21), the integral $F_{ijk}^A \to \int_0^r \frac{\phi^A(R)-\phi^A(0)}{r}\tilde{\mu}_{,i}dr$ from Eq. (23c) can be derived as follows:

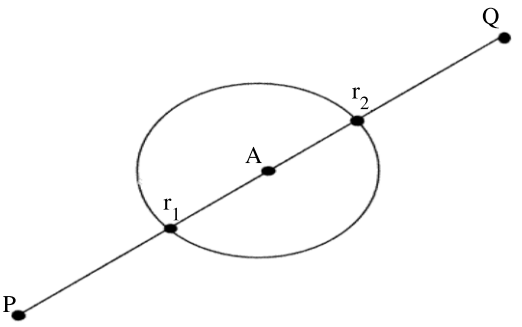

Fig. 4. Another special intersection.

For case 1: (exponential change of linear order)

Since $\tilde{\mu}_{,i} = c_i$ is constant for $\mu = \mu_0 e^{c_i x_i}$, the integral can be rewritten as follows: $c_i \int_0^r \frac{\phi^A(R)-\phi^A(0)}{r} dr$ and based on Eqs. (14) and (20), it can be derived that [19]:

$$\begin{aligned}\int_0^r \frac{\phi^A - \phi^A(0)}{r} dr = -\Bigg(&0.75r^4 + 12(d_A^2 + \bar{R}^2)rs - \frac{4}{3}d_A(8\bar{R}^2 + 2r^2 + 7rs + 3s^2)\sqrt{r^2 + 2sr + \bar{R}^2} \\ &+ 4r^3 s + 4sd_A(s^2 - 3\bar{R}^2)\ln\left(r + s + \sqrt{r^2 + 2sr + \bar{R}^2}\right) + 3r^2(d_A^2 + \bar{R}^2 + 2s^2) \\ &+ 8d_A\bar{R}^3 \ln\left(\bar{R}^2 + rs + \bar{R}\sqrt{r^2+2sr+\bar{R}^2}\right)\Bigg)\Big/ d_A^4 \end{aligned} \tag{37}$$

where r_1 and r_2 are the intersections between the line r and the circle centered at A with radius of d_A, as shown in Fig. 2.

For the expression as shown in Eq. (37), it should be noted that the special cases, $r + s + \sqrt{r^2 + 2sr + \bar{R}^2} = 0$ and $\bar{R}^2 + rs + \bar{R}\sqrt{r^2+2sr+\bar{R}^2} = 0$ may occur. In these cases, $s = -\bar{R}$, and $F_{ij}^A \to \int_0^r \phi^A(R)\tilde{\mu}_{,i} dr$ can be integrated as follows:

When $r + s + \sqrt{r^2 + 2sr + \bar{R}^2} = 0$, then $R = \bar{R} - r$, as shown in Fig. 3 and it can be derived that [19]:

$$\begin{aligned}\int_0^r \frac{\phi^A - \phi^A(\bar{R})}{r} dr = &\, r(36d_A^2(4\bar{R} - r) - 16d_A(18\bar{R}^2 - 9\bar{R}r + 2r^2) \\ &+ 3(48\bar{R}^3 - 36\bar{R}^2 r + 16\bar{R}r^2 - 3r^3))/(12d_A^4). \end{aligned} \tag{38}$$

When $\bar{R}^2 + rs + \bar{R}\sqrt{r^2+2sr+\bar{R}^2} = 0$, $R = r - \bar{R}$, as shown in Fig. 4 and it can be derived that [19]:

$$\begin{aligned}\int_0^r \frac{\phi^A - \phi^A(\bar{R})}{r} dr = &\, (r(36d_A^2(4\bar{R} - r) + 16d_A(18\bar{R}^2 - 9\bar{R}r + 2r^2) \\ &+ 3(48\bar{R}^3 - 36\bar{R}^2 r + 16\bar{R}r^2 - 3r^3)) - 192d_A\bar{R}^3 \ln(r))/(12d_A^4). \end{aligned} \tag{39}$$

For case 2: (linear)

Referring to Eq. (25) and let $a = \mu_0 + c_j x_j^p$, $b = c_j r_{,j}$, and then referring to Fig. 2, the radial integral can be derived based on Eqs. (14) and (20) that:

$$\begin{aligned}\int_0^r \frac{\phi^A(R) - \phi^A(\bar{R})}{r} \tilde{\mu}_{,i} dr = &\frac{c_i}{d_A^4}\Bigg(\frac{3r^2(a - 4bs) - 2br^3 + 8d_A R(-2a + b(r + 5s))}{2b^2} \\ &+ \frac{4d_A(2a^2 - 6abs + 3b^2(s^2 + \bar{R}^2))\ln\left(r + s + \sqrt{r^2 + 2sr + \bar{R}^2}\right) - 3r(a^2 - 4abs + 2b^2(d_A^2 + \bar{R}^2 + 2s^2))}{b^3} \\ &+ \frac{(3a^4 + 8b^4 d_A\bar{R}^3 - 12a^3 bs - 12ab^3(d_A^2 + \bar{R}^2)s + 6a^2b^2(d_A^2 + \bar{R}^2 + 2s^2))\ln(a + br)}{ab^4} \end{aligned}$$

$$-\frac{8d_A\bar{R}^3\ln\left(\bar{R}^2+rs+\bar{R}\sqrt{r^2+2sr+\bar{R}^2}\right)}{a}$$
$$+\frac{8d_A(a^2+b^2\bar{R}^2-2abs)^{\frac{3}{2}}\ln\left(b(\bar{R}^2+rs)-a(r+s)+R\sqrt{a^2+b^2\bar{R}^2-2abs}\right)-\ln(a+br)}{ab^3}\Bigg). \tag{40}$$

For the expression as shown in Eq. (40), it should be noted that the special cases, $r+s+\sqrt{r^2+2sr+\bar{R}^2}=0$ and $\bar{R}^2+rs+\bar{R}\sqrt{r^2+2sr+\bar{R}^2}=0$ may occur. In these cases, $s=-\bar{R}$ and $F_{ij}^A\to\int_0^r\phi^A(R)\tilde{\mu}_{,i}dr$ can be integrated as follows:

When $r+s+\sqrt{r^2+2sr+\bar{R}^2}=0$, then $R=\bar{R}-r$, as shown in Fig. 3 and it can be derived that:

$$\begin{aligned}\int_0^r\frac{\phi^A(R)-\phi^A(\bar{R})}{r}\tilde{\mu}_{,i}dr=(&c_i(-br(6a^2+ab(-16d_A+24\bar{R}-3r)\\&+2b^2(6d_A^2+18\bar{R}^2-6\bar{R}r+r^2+4d_A(r-6\bar{R})))\\&+2(3a^2+12b^3(d_A-\bar{R})^2\bar{R}+a^2b(12\bar{R}-8d_A)\\&+6ab^2(d_A^2-4d_A\bar{R}+3\bar{R}^2))\ln(a+br)))/(2b^4d_A^4).\end{aligned} \tag{41}$$

When $\bar{R}^2+rs+\bar{R}\sqrt{r^2+2sr+\bar{R}^2}=0$, then $R=r-\bar{R}$, as shown in Fig. 4 and it can be derived that:

$$\begin{aligned}\int_0^r\frac{\phi^A(R)-\phi^A(\bar{R})}{r}\tilde{\mu}_{,i}dr=(&c_i(-abr(6a^2+ab(16d_A+24\bar{R}-3r)\\&+2b^2(6d_A^2+18\bar{R}^2-6\bar{R}r+r^2+4d_A(6\bar{R}-r)))\\&-32b^4d_A\bar{R}^3\ln(r)+2(a+2b\bar{R})(3a^3+8b^3d_A\bar{R}^2+a^2b(6\bar{R}+8d_A)\\&+2ab^2(3d_A^2+4d_A\bar{R}+3\bar{R}^2))\ln(a+br)))/(2ab^4d_A^4).\end{aligned} \tag{42}$$

For case 3: (exponential change of secondary order)

Referring to Eq. (27) and let $a=c_i+c_{jk}(\delta_{ij}x_k^p+\delta_{ik}x_j^p)$, $b=c_{jk}(\delta_{ij}r_{,k}+\delta_{ik}r_{,j})$ then referring to Fig. 2 and based on Eqs. (14) and (20), it can be derived that:

$$\begin{aligned}\int_0^r\frac{\phi^A(R)-\phi^A(\bar{R})}{r}\tilde{\mu}_{,i}dr=\frac{1}{d_A^4}\Bigg(&-\frac{3br^5}{5}-\frac{3}{4}r^4(a+4bs)-4r(2bd_A\bar{R}^3+3a(\bar{R}^2+d_A^2)s)\\&-3r^2(2b(\bar{R}^2+d_A^2)s+a(\bar{R}^2+d_A^2+2s^2))-2r^3(2as+b(\bar{R}^2+d_A^2+2s^2))\\&+\frac{1}{3}d_AR(3b(r+s)(5\bar{R}^2+2r^2+4rs-3s^2)+4a(8\bar{R}^2+2r^2+7rs+3s^2))\\&+d_A(3b(\bar{R}^2-s^2)^2-4as(s^2-3\bar{R}^2))\ln\left(r+s+\sqrt{r^2+2sr+\bar{R}^2}\right)\\&-8ad_A\bar{R}^3\ln\left(\bar{R}^2+rs+\bar{R}\sqrt{r^2+2sr+\bar{R}^2}\right)\Bigg).\end{aligned} \tag{43}$$

For the expression as shown in Eq. (43), it should be noted that the special cases, $r+s+\sqrt{r^2+2sr+\bar{R}^2}=0$ and $\bar{R}^2+rs+\bar{R}\sqrt{r^2+2sr+\bar{R}^2}=0$ may occur. In these cases, $s=-\bar{R}$, and $F_{ij}^A\to\int_0^r\phi^A(R)\tilde{\mu}_{,i}dr$ can be integrated as:

When $r+s+\sqrt{r^2+2sr+\bar{R}^2}=0$, then $R=\bar{R}-r$, as shown in Fig. 3 and it can be derived that:

$$\begin{aligned}\int_0^r\frac{\phi^A(R)-\phi^A(\bar{R})}{r}\tilde{\mu}_{,i}dr=&-(0.6br^5+0.25(3a+8bd_A-12b\bar{R})r^4\\&+\frac{2}{3}(a(4d_A-6\bar{R})+3b(d_A^2-4d_A\bar{R}+3\bar{R}^2))r^3\\&-3(d_A-\bar{R})(2b(d_A-\bar{R})\bar{R}-a(d_A-3\bar{R}))r^2-12a(d_A-\bar{R})^2\bar{R}r)/d_A^4.\end{aligned} \tag{44}$$

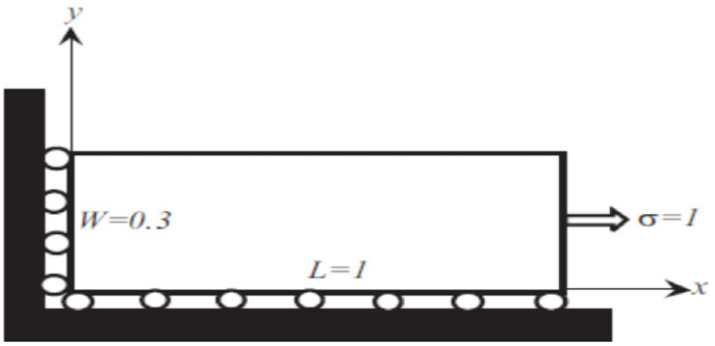

Fig. 5. Geometry and boundary conditions of 2D plate.

When $\bar{R}^2 + rs + \bar{R}\sqrt{r^2+2sr+\bar{R}^2} = 0$, then $R = r - \bar{R}$, as shown in Fig. 4 and it can be derived that:

$$\begin{aligned}\int_0^r \frac{\phi^A(R) - \phi^A(\bar{R})}{r}\tilde{\mu}_{,i}dr = {} & (4\bar{R}(-4bd_A\bar{R}^2 + 3a(d_A+\bar{R})^2)r \\ & + 3(d_A+\bar{R})(2b\bar{R}(d_A+\bar{R}) - a(d_A+3\bar{R}))r^2 \\ & + \frac{2}{3}(a(4d_A+6\bar{R}) - 3b(d_A^2+4d_A\bar{R}+3\bar{R}^2))r^3 \\ & + 0.25(-3a+8bd_A+12b\bar{R})r^4 - 0.6br^5 - 16ad_A\bar{R}^3\ln(r))/d_A^4. \end{aligned} \quad (45)$$

Substituting these analytical expressions into Eqs. (15) and (18) and then substituting Eq. (11) into the above equation and the results into Eqs. (4) and (8) for boundary and internal points, one can establish the desired system of equations. It should be noted that the expressions of Eqs. (24)–(45) are suitable for solving both 2D and 3D problems.

5. Numerical examples

A computer code called RIBEM (radial integration BEM) has been developed using the formulations derived in this paper. To verify the correctness of the derived formulations, three numerical examples are presented in the following.

5.1. Stresses over a 2D rectangular plate

The first example to be considered is an isotropic, continuously non-homogeneous elastic rectangular plate with the dimensions $L \times W$ as shown in Fig. 5. The investigated plate is subjected to a uniform tensile stress loading $\sigma = 1$.

The boundary of the plate is discretized into 52 equally-spaced linear boundary elements: 20 along longitudinal and 6 along transversal directions. 95 internal nodes are used as shown in Fig. 6. Poisson's ratio is selected as $\nu = 0.25$ and an exponential variation of shear modulus in the transversal y direction is used, which is described by

$$\mu = \mu_0 e^{\beta y}, \qquad \beta = \frac{1}{W}\ln\left(\frac{\mu_W}{\mu_0}\right)$$
$$\mu_0 = 4000, \qquad \mu_W = 8000.$$

For comparison, this problem is also computed using the FEM software ANSYS. Fig. 7 shows the computed displacement component u_1 over the top-side, while Fig. 8 shows the computed stress σ_{11} along the middle line $x = 0.5$ of the plate and Fig. 9 shows a plot of the results.

From Figs. 7–9, it can be seen that the RIBEM results are very close to the FEM solutions. This demonstrates that the derived analytical expressions are correct for this example. In this example, the computational time using numerical solution is 4 s, while RIBEM takes 2 s. About 50% of computational time is saved.

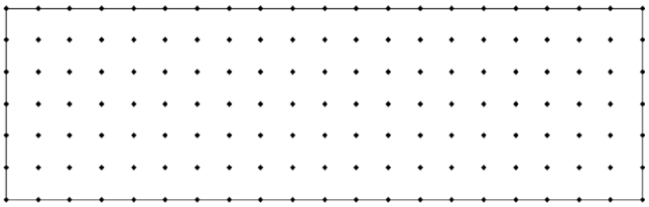

Fig. 6. BEM model of the plate.

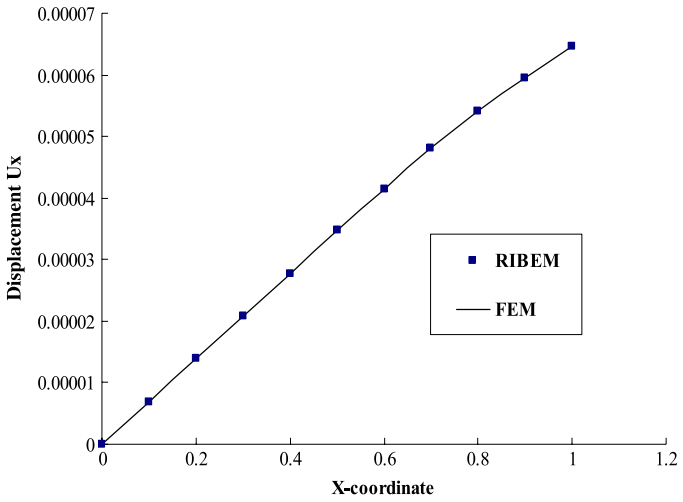

Fig. 7. Displacement distribution along top-side of the plate.

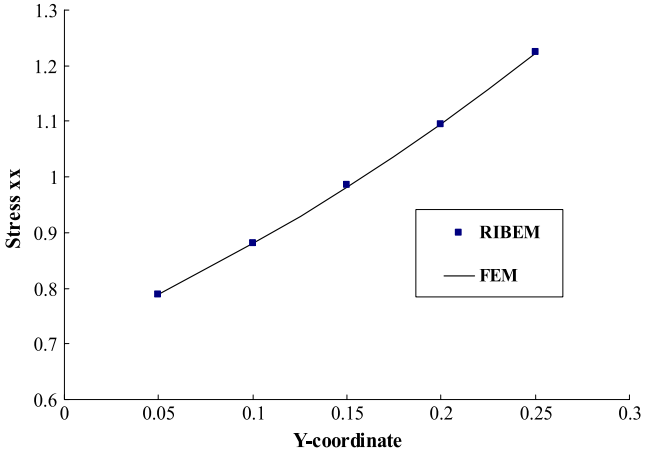

Fig. 8. Stress σ_{11} distribution along middle line of the plate.

5.2. Stress over a 3D hexahedral

The second example is a 3D hexahedral elastic analysis. Fig. 10 shows the dimensions and boundary conditions of the hexahedral structure. The bottom surface of the composite model is fixed, while the top surface of the hexahedral is subjected to a pressure of 100 units and others are traction free. Poisson's ratio is selected as $\nu = 0.25$.

An exponential variation of shear modulus along the z direction is assumed, which is described as follows:

$$\mu = \mu_1 e^{\gamma z^2}, \qquad \gamma = \frac{1}{H^2} \ln \frac{\mu_2}{\mu_1}$$

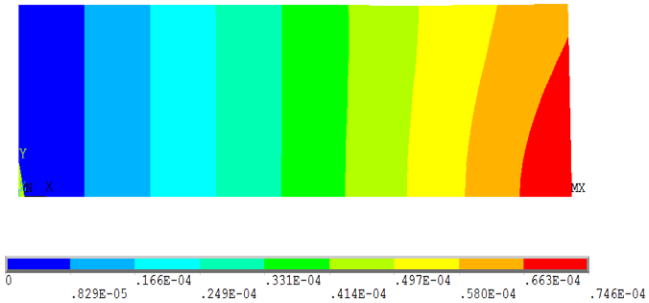

Fig. 9. x-direction displacement contour of the plate.

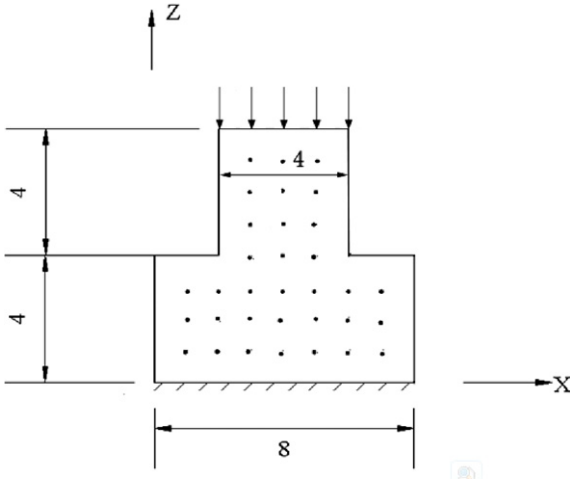

Fig. 10. Dimensions and boundary conditions of the hexahedral.

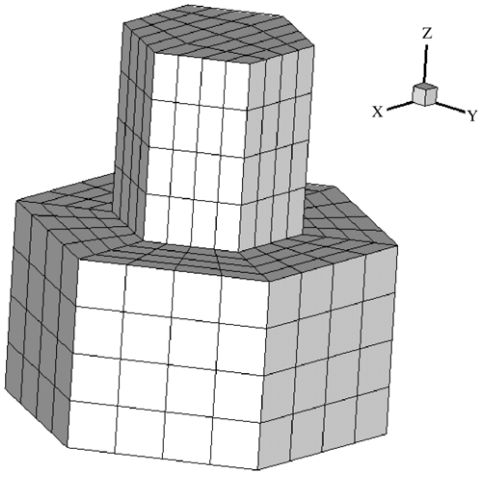

Fig. 11. BEM model of the hexahedral.

in which $H = 8$ being the height of the hexahedral, $\mu_1 = 4000$ and $\mu_2 = 8000$ being the shear modulus on the bottom and top sides of the hexahedral, respectively.

The BEM model is shown in Fig. 11, which consists of 448 linear boundary elements and 655 nodes, among which the number of boundary and internal nodes are 450 and 205, respectively. The displacements at 7 internal points alone

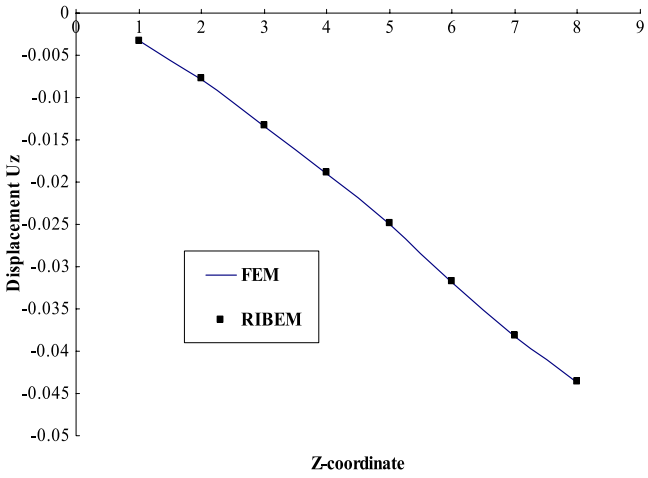

Fig. 12. Computed displacement for the hexahedral.

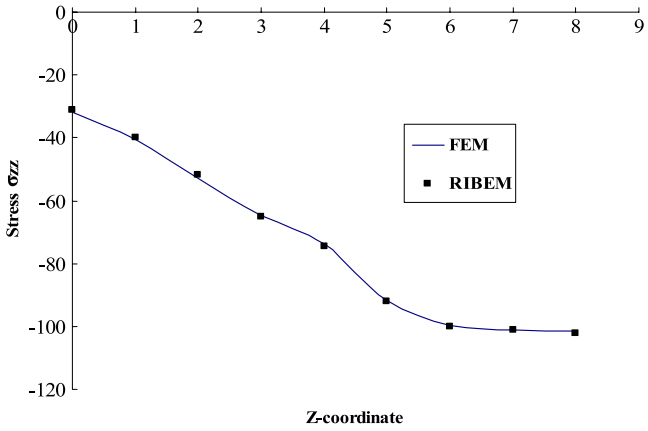

Fig. 13. Computed stress σ_{zz} of the hexahedral.

the z direction are investigated, which are located at the line of $x = 0$, $y = 0$ as shown in Fig. 10. For comparison, the problem is also computed using the FEM software ANSYS. Fig. 12 shows the computed results using RIBEM and FEM for the 7 internal points, while Fig. 13 shows the computed stress σ_{zz} along the z direction midline of the hexahedral and Fig. 14 shows a plot of the z direction displacement contour.

From Figs. 12–14, it can be seen that the presented RIBEM results are in good agreement with FEM results, although coarse meshes are used in BEM. In addition to be sure, the displacements computed using FEM are similar to those using the current RIBEM with the same coarse meshes as in RIBEM, but the accuracy of stresses using FEM is worse than using RIBEM. Therefore, to achieve a same accurate stress results, a finer mesh is necessary for FEM. This demonstrates the advantage of RIBEM over FEM in meshing aspect.

In this example, the computational time using numerical solution is about 25 min, while RIBEM takes about 6 min. This means that more than 75% computational time is saved.

5.3. Stress over a 3D cube

To test the computational efficiency of the presented method, the third example is a 3D cube elastic analysis. Fig. 15 shows the BEM model of the cube with the dimensions of $10 \times 10 \times 10$. The bottom surface of the model is fixed, while the top surface of the cube is subjected to a pressure of 100 units and others are traction free. The linearly varying shear modulus along the z-direction is $\mu = \mu_1 + rz$, where $r = \frac{1}{H}(\mu_2 - \mu_1)$ with $H = 10$ being the height

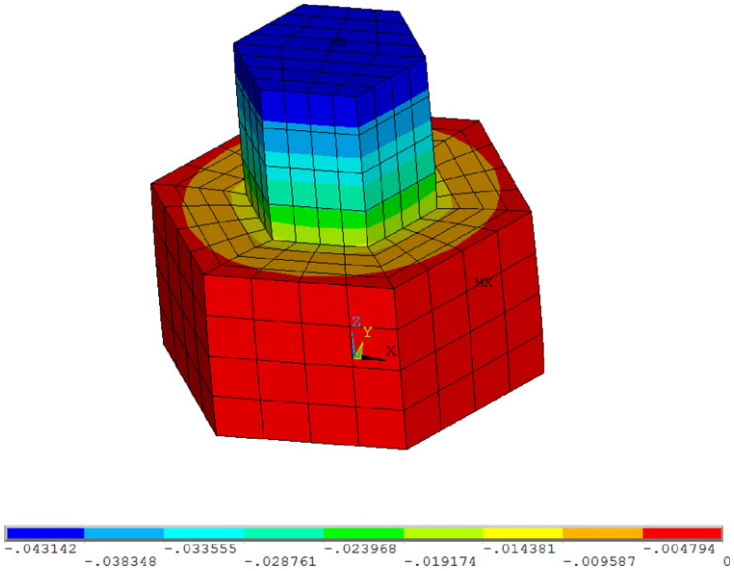

Fig. 14. Displacement contour of the results.

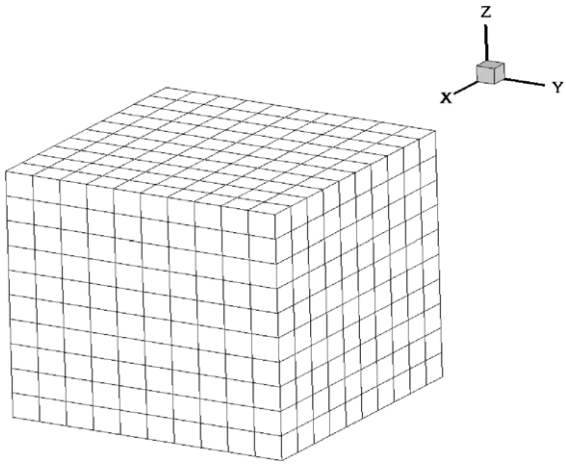

Fig. 15. BEM model of the cube.

of the cube, $\mu_1 = 4000$ and $\mu_2 = 8000$ being the shear modulus on the bottom and top sides of the cube, respectively and Poisson's ratio is also selected as $\nu = 0.25$.

The BEM model is shown in Fig. 15, which consists of 600 linear boundary elements and 1331 nodes, among which the number of boundary and internal nodes are 602 and 729, respectively. The displacements at 9 internal points are investigated, which are located at the line of $x = 5$, $y = 5$. For comparison, the problem is also computed using the FEM software ANSYS. Fig. 16 shows the computed displacement results using RIBEM and FEM for the 9 internal points, while Fig. 17 shows the computed stress σ_{zz} along the z direction midline of the cube and Fig. 18 shows a plot of the z direction displacement contour.

From Figs. 16–18, it can be seen that the presented RIBEM results are in good agreement with FEM results, although coarse meshes are used in both BEM and FEM. In this example, the computational time spent in numerical solution is about 176 min, while RIBEM takes about 37 min, nearly 80% computational time is saved. It is expected that more computational time can be saved using the present method for larger engineering problems.

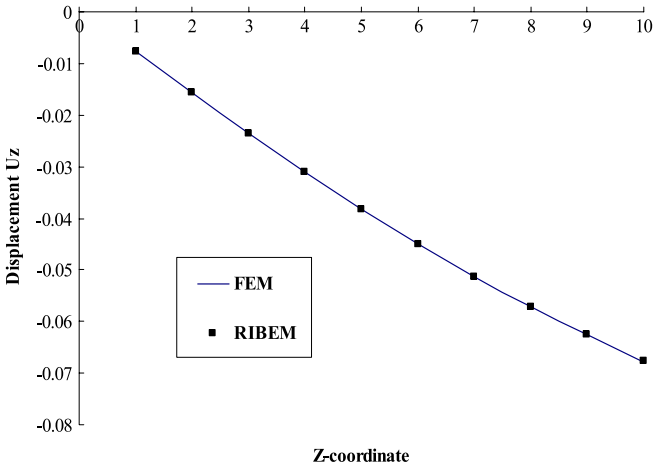

Fig. 16. Computed displacement for the cube.

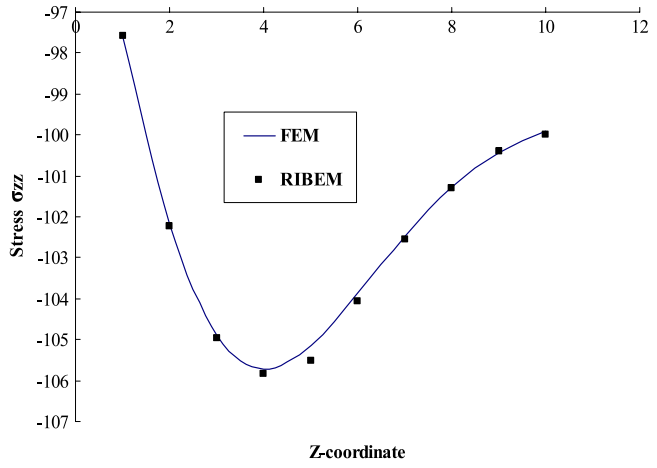

Fig. 17. Computed stress σ_{zz} of cube.

6. Conclusion

An efficient boundary element analysis approach is presented for solving elastic stress problems with several kinds of variable shear modulus. The radial integration method is used to transform the domain integrals appearing in the stress boundary-domain integral equations into boundary integrals. The radial integral in RIM with several kinds of variable shear modulus is analytically integrated for domain integrals based on the employment of the compactly supported fourth-order spline RBF. The strong singularity involved in the stress integral equation is explicitly removed for the derivation of the analytical expressions. The derived formulation can save computational time considerably in forming non-homogeneous integral coefficients.

For the use of the RIBEM to solve other problems [8,16], the final radial integrals can be classified into the evaluation of line integral as shown in Eq. (23), and the integration results Eqs. (24)–(45) can be applied to solve a broad range of engineering problems, not just limited to elastic problems.

Acknowledgment

The authors gratefully acknowledge the National Natural Science Foundation of China for financial support to this work under Grant NSFC Nos. 11172055 and 11202045.

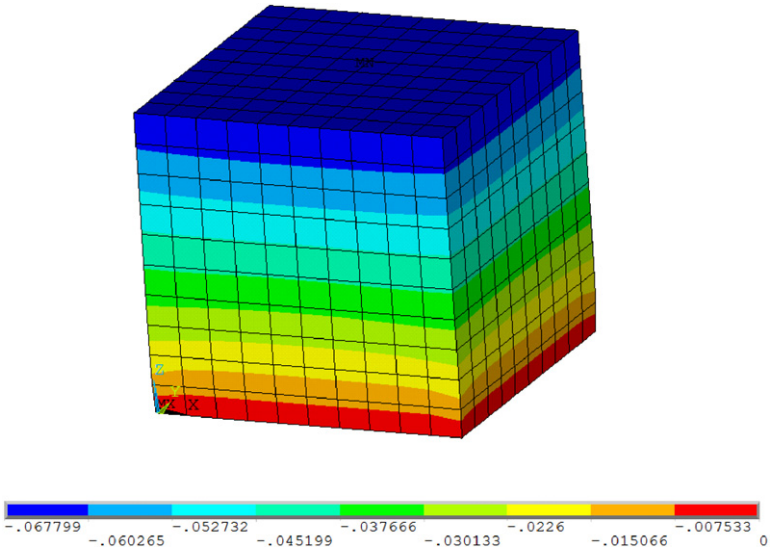

Fig. 18. Displacement contour of the results.

References

[1] J. Sladek, V. Sladek, S.N. Atluri, Local boundary integral equation (LBIE) method for solving problems of elasticity with nonhomogeneous material properties, Comput. Mech. 24 (2000) 456–462.
[2] P.W. Partridge, C.A. Brebbia, L.C. Wrobel, The Dual Reciprocity Boundary Element Method, Computational Mechanics Publications, Southampton, 1992.
[3] X.W. Gao, The radial integration method for evaluation of domain integrals with boundary-only discretization, Eng. Anal. Bound. Elem. 26 (2002) 905–916.
[4] X.W. Gao, A boundary element method without internal cells for two-dimensional and three-dimensional elastoplastic problems, J. Appl. Mech. 69 (2002) 154–160.
[5] X.W. Gao, Evaluation of regular and singular domain integrals with boundary-only discretization—theory and Fortran code, J. Comput. Appl. Math. 175 (2005) 265–290.
[6] X.W. Gao, An effective method for numerical evaluation of general 2D and 3D high order singular boundary integrals, Comput. Methods Appl. Mech. Engrg. 199 (2010) 2856–2864.
[7] Ch. Zhang, M. Cui, J. Wang, X.W. Gao, 3D crack analysis in functionally graded material, Eng. Fract. Mech. 26 (2002) 119–132.
[8] K. Yang, X.W. Gao, Radial integration BEM for transient heat conduction problems, Eng. Anal. Bound. Elem. 34 (2010) 557–563.
[9] X.W. Gao, Ch. Zhang, L. Guo, Boundary only element solutions of 2D and 3D nonlinear and nonhomogeneous elastic problems, Eng. Anal. Bound. Elem. 31 (2007) 974–982.
[10] X.W. Gao, Ch. Zhang, J. Sladek, V. Sladek, Fracture analysis of functionally graded materials by a BEM, Compos. Sci. Technol. 68 (2008) 1209–1215.
[11] C.Y. Dong, C.J. Pater, A boundary-domain integral equation for a coated plane problem, Mech. Res. Commun. 27 (2000) 643–652.
[12] G.Z. Xie, F.L. Zhou, J.M. Zhang, X.S. Zheng, C. Huang, New variable transformations for evaluating nearly singular integrals in 3D boundary element method, Eng. Anal. Bound. Elem. 37 (2013) 1169–1178.
[13] R.P. Shaw, G.S. Gipson, A BIE formulation of a linearly layered potential problem, Eng. Anal. Bound. Elem. 16 (1995) 1–3.
[14] A. Sutradhar, G.H. Paulino, Transient heat conduction in homogeneous and non-homogeneous materials by the Laplace transform Galerkin boundary element method, Eng. Anal. Bound. Elem. 26 (2002) 119–132.
[15] J.T. Chen, H.K. Hong, Review of dual boundary element methods with emphasis on hypersingular integrals and divergent series, Appl. Mech. Rev. 52 (1999) 17–33.
[16] K. Yang, X.W. Gao, Y.F. Liu, Using analytical expressions in radial integration BEM for variable coefficient heat conduction problems, Eng. Anal. Bound. Elem. 35 (2011) 1085–1089.
[17] X.W. Gao, A meshless BEM for isotropic heat conduction problems with heat generation and spatially varying conductivity, Internat. J. Numer. Methods Engrg. 66 (2006) 1411–1431.
[18] X.W. Gao, K. Yang, Interface integral BEM for solving multi-medium elasticity problems, Comput. Methods Appl. Mech. Engrg. 198 (2009) 1429–1436.
[19] K. Yang, Y.F. Liu, X.W. Gao, Analytical expressions for evaluation of radial integrals in stress computation of functionally graded material problems using RIBEM, Eng. Anal. Bound. Elem. 44 (2014) 98–103.
[20] X.W. Gao, T.G. Davies, Boundary Element Programming in Mechanics, Cambridge University Press, Cambridge, 2002.